Title: “Morphogen gradients applied basally to human embryonic stem cells to control and dissect tissue patterning"

Tom Wyatt*[3,5], Mingfeng Qiu*[2,4], Julie Stoufflet*[1], Hassan Omais[1], Gabriel Thon[1,3], Sara Bonavia[3], Pascal Hersen[1], Vincent Hakim[2] & Benoit Sorre[1,3]

1 - Physics of Cells and Cancer, Institut Curie, Université PSL, Sorbonne Université, CNRS UMR168, 75005 Paris, France

2 - Laboratoire de Physique de l’Ecole Normale Supérieure, CNRS, Ecole Normale Supérieure, PSL University, Sorbonne Université, Université Paris-Cité, Paris, France

3 -Laboratoire "Matière et Systèmes Complexes" (MSC), CNRS UMR 7057, Université Paris Cité, CNRS, Paris, France

4 - School of Mathematics and Statistics, University of Canterbury, Christchurch, New Zealand.

5 – present address : Cyclana Bio, Babraham Research Campus, Cambridge, UK

* Equal contributions

Abstract

Morphogen gradients are used repeatedly during development to pattern embryonic tissues. Absolute concentrations, duration or even temporal derivative of morphogen concentration have all been proposed to carry positional information. However, establishing the causal relationship between the gradient spatio-temporal profile and resulting cellular diversity and tissue patterning is difficult to address in live embryos because of lack of tools to control those variables.

Here, we developed microfluidics devices able to apply spatio-temporally well-defined morphogen landscapes on the basal side of human embryonic stem cells colonies, thus mimicking how BMP4 is delivered to the pluripotent epiblast during mouse gastrulation. Combining live imaging and theoretical modelling, we show that in this configuration the absolute concentration of BMP4 provides positional information and the cell identities emerging during differentiation can vary according to the shape of the gradient.

Our toolbox provides a powerful means to dissect the logic of patterning and to engineer tissues precisely.

Introduction

In mammalian embryos, gastrulation is the process during which cells of the pluripotent epiblast are allocated into three germ layers (ectoderm, mesoderm and endoderm) and the body plan is laid out. In the mouse embryo, gastrulation is initiated by BMP4 secreted by the Extra Embryonic Ectoderm (ExE) which creates a concentration gradient on the posterior proximal side of the adjacent epiblast[1]. In response to BMP4 stimulation, epiblast cells start to produce secondary morphogens such as WNT and NODAL, initiating the formation of the Primitive Streak (PS), a structure that extends on the posterior side of the embryo as gastrulation proceeds and from which mesoderm and endoderm emerge, see Fig.1AB. It has been challenging to disentangle the complex interactions between key signalling pathways driving gastrulation and to establish the causality link between their spatio-temporal dynamics and the resulting patterning of the PS[2,3]. This is partly due to the difficulty of observing the embryos at those stages for technical reasons as well as ethical reasons in case of Human, but also to the lack of tools to manipulate signalling landscapes with sufficient spatio-temporal resolution.

Recently, BMP4 stimulated human Embryonic Stem Cell (hESC) colonies that are confined in 2D on micropatterned substrates and self-organise in concentric rings of the 3 germ layers (h-2D-gastruloids) have emerged as an elegant solution to the accessibility issue[4]. The patterning relies on self-organisation of BMP signalling which is gradually restricted to the edge of the colonies despite homogenous stimulation. This system has permitted to observe and dissect the BMP→WNT→ NODAL signalling cascade at play[2,5–7]. However, it does not allow to take control of the spatio-temporal dynamics of BMP signalling in the colony. Microfluidic delivery of an apical gradient of BMP4 over colonies could break the radial symmetry of patterning but didn't prevent self-organisation[8,9]. One important factor in this self-organisation is the loss of accessibility of the apically provided BMP4 molecules to the BMP receptors located on the basolateral side of the tissue, below tight junctions[10]. In the mouse embryo, for example, ExE secreted BMP4 forms a concentration gradient on the basal side of epiblast cells as it diffuses in the basal lamina between the epiblast and the visceral endoderm, Fig.1AB[9].

We hypothesised that this configuration could be crucial to define how the morphogen is perceived. Thus, to mimic the *in vivo* situation, we have developed two novel microfluidic devices capable of stimulation of hESC tissue on their basal side with high spatio-temporal resolution. Under static parabolic gradients of BMP4 we have observed a sharp and reproducible pattern of only three cell identities with both fate transitions happening at constant BMP4 concentrations. By contrast, stimulation by a step gradient of BMP4 permitted emergence of the endoderm while this identity was not observed in parabolic gradients. Combining live reporters of signalling activities in the tissue and mathematical modelling, we explain these different behaviours by the dynamics of signalling and especially a bistability in WNT/NODAL signalling, which is strongly constrained by our observations.

Results

A microfluidic device for basal stimulation of hESCs with controlled spatio-temporal profiles of morphogens.

We designed a two-layer microfluidic chip, in which BMP4 is presented on the cells basal side, through a porous membrane. The top compartment is composed of a microfluidic circuit generating a parabolic gradient of BMP4 concentration in the downstream culture chamber by successive mixing of media inputs, Fig.1D. This parabolic gradient is achieved if one of the side inputs is fed with a medium containing BMP4 while the two others are fed with base medium alone, with equal flow rates. Depending on the configuration of media inputs, linear, dumbbell or even antiparallel gradients of two morphogens can be generated with the same design[11] see Fig1, Fig.S1, movie 1 and methods.

We verified using fluorescently tagged dextran of a molecular weight comparable to BMP4 (40kDa) that the gradient had a parabolic profile in agreement with the theoretical one (Fig.1FG). As gradient generation does not rely on diffusion, a stable gradient was created in under 1 minute and was stable as long as the flow was maintained, Fig.1D-G & movie 1.

To achieve homogenous and efficient response to BMP4 stimulation, we found that high porosity membranes such as anopore aluminium oxide membranes were necessary, see methods and Fig.S1. As methods commonly used to incorporate membranes in microfluidic devices[12,13] could not be used with these membranes, we have adapted multilayer soft lithography thermal bonding[14] to robustly attach the gradient-generating PDMS chip to anopore membranes. To that end, the membranes were first stamped with a thin layer of PDMS to block the pores everywhere except on a rectangular window matching the size of the gradient chamber of the top layer chip[15]. After partial curing, the microfluidic gradient-generating chip was aligned on the stamped membrane and the assembly further cured for irreversible bonding, see Fig.S1A and methods.

A monolayer of hESCs was seeded on the membrane on the opposing side of the gradient window, in the bottom compartment of the device (Fig.S1BC, movie 1 and Methods). hESCs were able to grow and maintain pluripotency in the device for at least 72 hours. We first applied a parabolic gradient of BMP4 ($[BMP4]_{max}$ = 5ng/ml) on the basal side of hESC colonies and assayed cell response by immuno-fluorescence (IF) against phospho-SMAD1, an effector of the pathway immediately downstream of the receptor[16], Fig.1C. 6 hours after initiation of stimulation, a graded pSMAD1 signal was observed along the BMP4 gradient. Quantification showed that the response profile was reproducible across replicates and followed quantitatively the expected profile given the parabolic BMP4 gradient and the measured dose-response of isolated cells Fig.1HI and S1D. The same quantification after 24 hours of stimulation yielded a similar pSMAD1 profile, Fig.1J. Together, these experiments show that, unlike in apical stimulation experiments where cells' response to BMP4 self-organises to restrict itself at the edge of the colonies after 24 hours[8–10], basal gradient stimulation allows one to impose a spatio-temporal profile of BMP stimulation on a colony of hESCs because it preserves accessibility to BMP receptors over time.

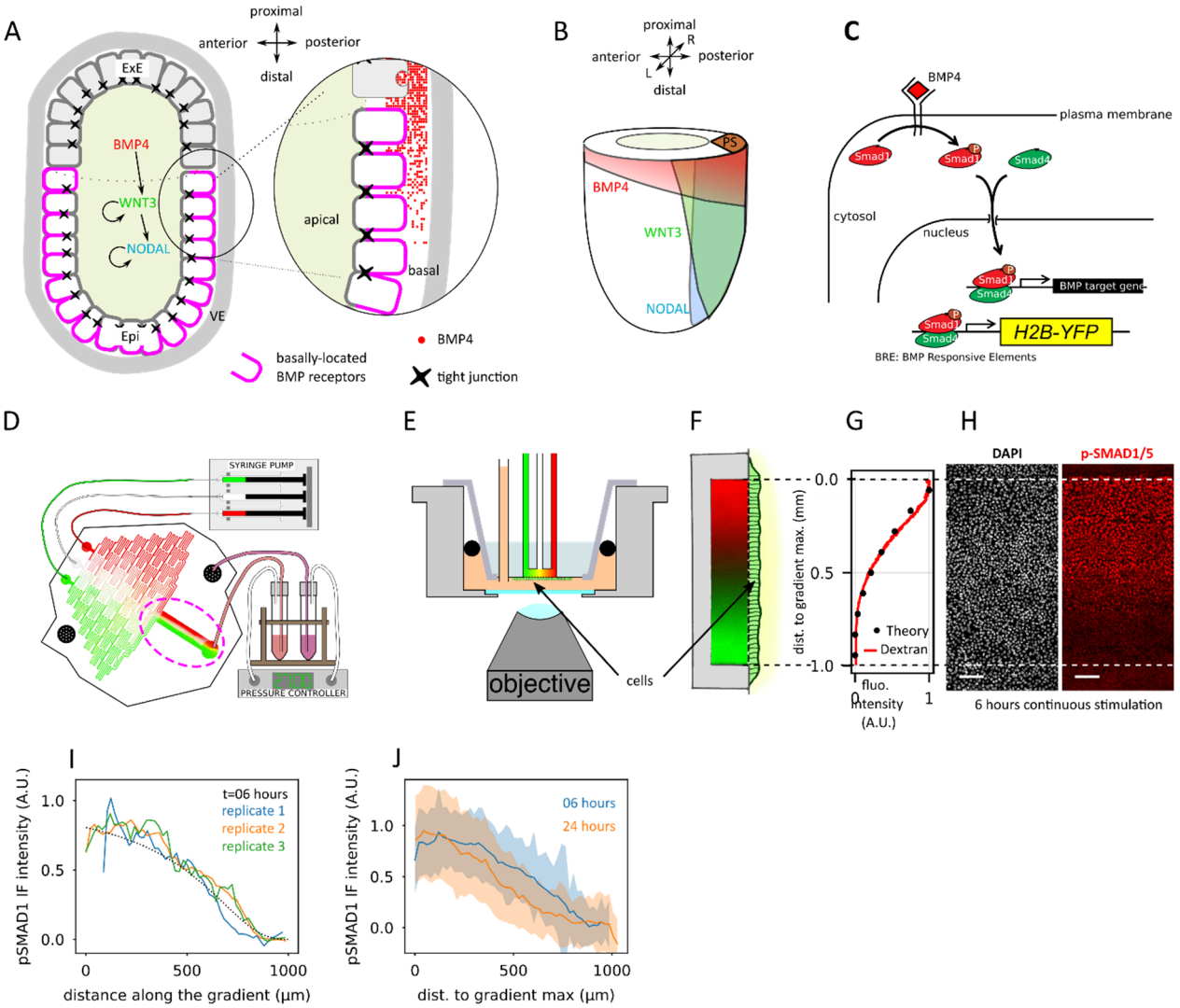

Figure 1: basal stimulation allows to impose a stable gradient of BMP activity on an hESC colony

A) *Schematic representation of a sagittal section of the mouse embryo at the start of gastrulation (E5.5-E6). BMP4 molecules secreted by the Extra Embryonic Ectoderm (ExE) start a signalling cascade in the adjacent Epiblast (Epi). VE: Visceral Endoderm. Right: close up view revealing the apico-basal polarity of epiblast cells and the restriction of BMP receptors on the basal cells (purple lines). Only the BMP4 molecules present on the basal side of epiblast cells have access to the receptors. They form a proximo-distal gradient in the basal lamina between the epiblast and the surrounding visceral endoderm. Adapted from*[9].

B) *Resulting signalling landscape in the mouse epiblast at mid-gastrulation (E7.0) adapted from*[17]*. Fate mapping experiments have shown that cells emerging early on from the proximal/posterior region of the PS will migrate proximally to form extra-embryonic mesoderm or laterally to form early embryonic mesoderm derivatives, whereas cells emerging later, i.e. distally to the source of BMP4, will form axial mesoderm and definitive endoderm.*

C) *Simplified representation of the BMP signalling cascade. Binding of BMP ligands to their receptor triggers the phosphorylation of SMAD1/5 which then associates with SMAD4 and translocates into the nucleus where the complex binds to DNA through BMP Responsive Elements (BRE) to modulate the expression of its target genes. These BRE have been cloned into a transgenic fluorescent reporter system stably integrated in the genome of hESCs by a PiggyBAC transposase.*

D) *General principle diagram of the device. Through successive mixing of 3 media pushed at a constant flow rate in the chip by a syringe pump, a smooth concentration gradient is generated in the rectangular chamber, inside the dotted*

purple ellipse. A pressure controller sets pressures on the apical and basal sides of the tissue independently to prevent bubble appearance and tissue detachment from the membrane.

E) *Cross section of the gradient chip in its observation cuvette. The morphogen gradient is established in the top compartment while cells are in the bottom compartment. Cells adhere to the porous membrane through which they sense the gradient on their basal side.*

F) *Close-up view on the region of the chip where cells are seeded. Rotated by 90° compared to panel E. Parabolic antiparallel gradients in the chip are visualized with green and red fluorescent dextrans (40kDa).*

G) *Quantification of the red dextran gradient (red curve) showing good agreement with the theoretical parabolic profile (black dots).*

H) *Immuno-fluorescence (IF) of hESC tissue for pSMAD1/5 after 6 hours of stimulation with a parabolic BMP4 gradient ($[BMP4]_{max}$=5ng/ml).*

I) *Quantification of pSMAD1 intensity of individual cells as a function of their position in the BMP4 gradient, after 6 hours. Average fluorescence profiles of 3 independent replicates are displayed, showing reproducibility. The dotted line corresponds to the expected pSmad1 profile given a parabolic BMP4 gradient and the measured dose-response curve to BMP4 stimulation of hESCs in sparse cultures:* $pSMAD1 = \frac{[BMP4]^n}{K_{pSMAD1}^n + [BMP4]^n}$ with $K_{pSMAD1} = 0.82ng/ml\,, n = 1.36$.

J) *Comparison of the pSMAD1 profiles at 6 and 24 hours. Solid lines are the average fluorescence of individual cells from 3 and 5 independent experiments at 6 and 24 hours, respectively. Shaded areas represent the standard deviation of the cell populations (n=17x10^3 and 47 x10^3 cells in 3 and 5 replicates respectively)*

Scale bars: 100µm.

hESCs can interpret absolute concentration of basal BMP4 stimulation.

We investigated how the hESC colony would differentiate under a static parabolic gradient with $[BMP4]_{max}$ = 5ng/ml. To reveal the cell identities in real time, we used the Germ Line Reporter (GLR) RUES2 hESC subclone engineered to express fluorescent reporters under the control of genes characteristic of the 3 germ layers: SOX2-mcitrine for pluripotent cells, TBXT-2A-mCerulean for the PS/mesoderm, and SOX17-2A-tomato for the endoderm, hereafter abbreviated as SOX2-YFP, TBXT:CFP and SOX17:RFP[18], respectively, Fig.2A.

Initially all cells were positive for SOX2-YFP, consistent with their pluripotent identity. During the first day of stimulation, SOX2-YFP disappeared at the higher half of the gradient. After 36-42 hours, TBXT:CFP started to be detected in a band of $SOX2^-$ cells adjacent to the $SOX2^+$ domain (Figs.2B,S2 and movie 2). After 72 hours of stimulation, further characterization with IF revealed that [$SOX2^-$/$TBXT^-$] cells at the higher end of the gradient were positive for CDX2 indicating an amnion-like cell identity as observed in other BMP4-induced hESC differentiation systems[19–24]. $TBXT^+$ cells were also positive for CDX2, indicating a proximal derivative of the PS identity such as extraembryonic mesoderm[25], also reported after BMP4 stimulation of hESCs and mouse epiblast like cells[26–29]. Characterization of cell identity at the single cell level showed that each domain was composed of an almost pure population of cells with sharp boundaries, Figs.2CD,S2EF.

We then asked how the observed pattern depended on gradient properties. Increasing the maximal concentration while keeping the parabolic shape of the gradient induced a shift of the position of the band of $TBXT^+$ cells, Fig.2EF. Converting the position of the boundaries between the domains into BMP4 concentration showed that, within experimental precision, fate transition occurred at a constant concentration, Fig.2G. At $[BMP4]_{max}$ = 1.25ng/ml the [$TBXT^-$/$CDX2^+$] domain was not induced but $TBXT^+$

167 domain was still present showing that the presence of the [TBXT$^-$/CDX2$^+$] domain is not necessary to induce
168 the TBXT$^+$ cell identity. As in other systems, the emergence of TBXT$^+$ cells was dependant on WNT signalling
169 as the band disappeared in the presence of WNT secretion inhibitor IWP2, Fig.S2G.

170 These experiments show that in static BMP4 gradients, cells can interpret absolute BMP4 concentration to
171 generate 3 domains with sharp boundaries at constant concentration thresholds. The TBXT$^+$ cells appeared
172 between 1.0±0.1 and 1.7 ±0.2 ng/ml *i.e.* in the linear range of the dose response of cells to BMP4 (Fig.S1).
173 This value must be compared to the 50ng/ml BMP4 typically used to elicit similar fates with apical
174 stimulation[4,8]. Another important difference with apically stimulated systems is that the repertoire of
175 accessible fates in a static basal gradient is restricted to only 3 identities. Indeed, no SOX17$^+$ cells were
176 observed in the static gradient while almost all derivatives of PS observed in h2D-Gastuloids[30]. SOX17$^+$ cells,
177 mixed with TBXT$^+$ cells, were nevertheless observed, but outside the stimulation area at the edge between
178 the high end of the gradient and the unstimulated zone, where the tissue experiences a step gradient of
179 BMP4 concentration Figs.2B,S2AB & movie S2.

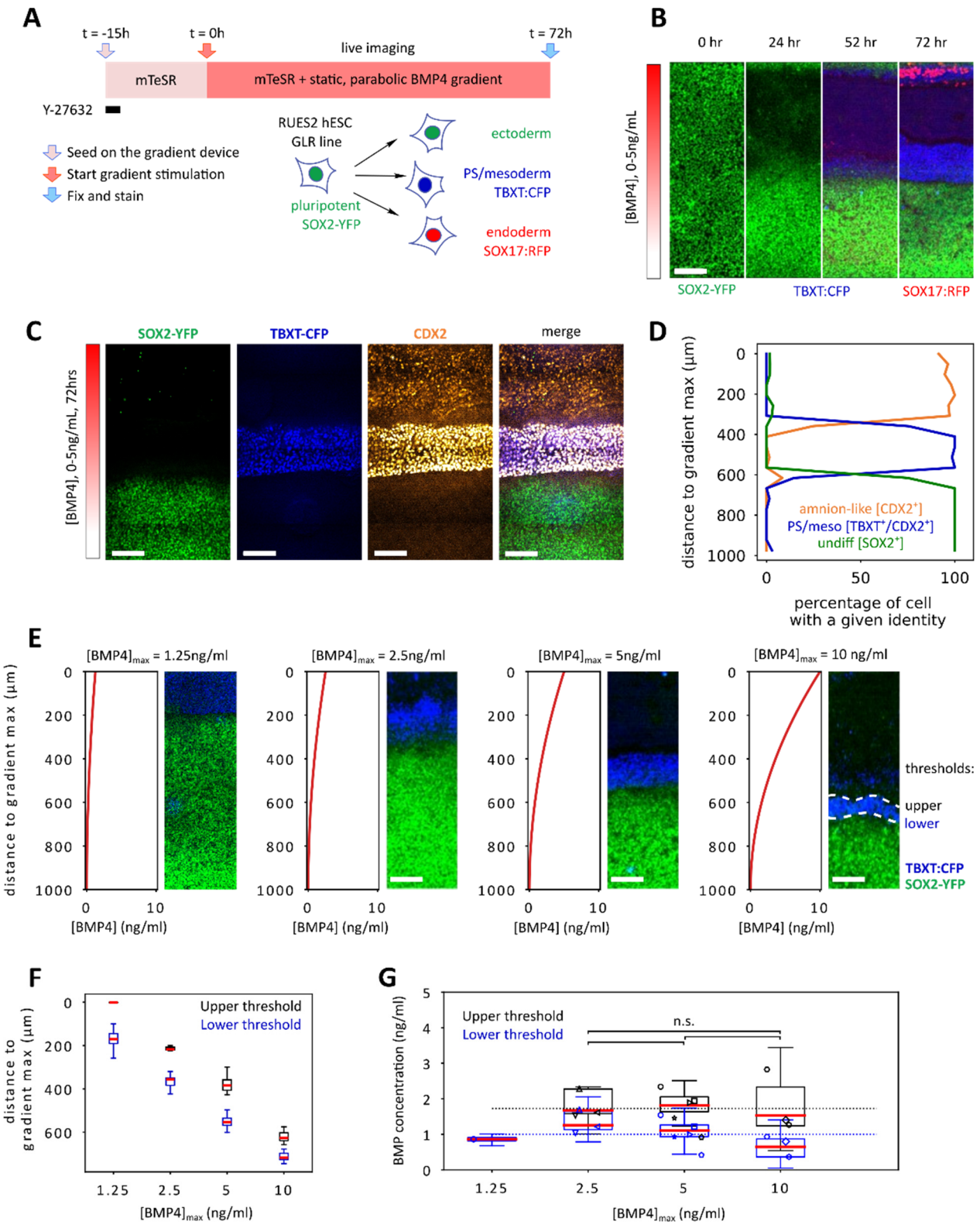

Figure 2: pattern of differentiation of hESCs in a static parabolic gradient of BMP4

A) *Presentation of the experimental timeline (top left) and of the Germ Layer Reporter (GLR) RUES2 hESC cell line we used in this figure. This cell line has been engineered to report cell identities with the following fluorescent proteins: SOX2-mCitrine (SOX2-YFP) for pluripotency, TBXT-2A-mCerulean (TBXT:CFP) for Primitive Streak (PS)/mesoderm and SOX17-2A-tdTomato (SOX17:RFP) for endoderm.*

186 ***B)*** *Temporal evolution of the SOX2-YFP, TBXT:CFP and SOX17:RFP reporters over 72 hours of differentiation in the static*
187 *parabolic gradient of BMP4 with* $[BMP4]_{max}$ *= 5ng/ml.*

188 ***C)*** *Representative images for the SOX2-YFP, TBXT:CFP and IF for CDX2 after 72 hours in a static parabolic gradient of*
189 *BMP4 with* $[BMP4]_{max}$ *= 5ng/ml.*

190 ***D)*** *Quantification of the percentage of the cells classified as undifferentiated* $[SOX2^+/TBXT^-/CDX2^-]$ *PS/mesoderm*
191 $[SOX2^-/TBXT^+/CDX2^+]$ *and extraembryonic/amnion-like* $(SOX2^-/ TBXT^-/ CDX2^+)$ *along the gradient for one experiment.*

192 ***E)*** *Evolution of the position of the band of* $TBXT^+$ *cells at t=72 hours for 4 values of* $[BMP4]_{max}$. *The theoretical BMP4*
193 *concentration profiles are depicted on the left.*

194 **F)** Quantification of *evolution of the upper and lower thresholds of the band of* $TBXT^+$ *cells at t=72 hours for 4 values*
195 *of* $[BMP4]_{max}$. *The box plots represent the variability of the position of the thresholds.*

196 ***G)*** *Evolution of BMP4 concentration at the position of upper and lower thresholds of the band of* $TBXT^+$ *cells as a*
197 *function of* $[BMP4]_{max}$. *Red bars represent the median and box plots represent the variability of thresholds position of*
198 *all replicates for a given* $[BMP4]_{max}$. *Pairs of black and blue symbols represent the median position of upper and lower*
199 *thresholds for individual replicates. p-values were calculated using the medians of individual replicates (n=3,5,3 for*
200 $[BMP4]_{max}$ *= 2.5, 5, 10 ng/ml respectively). For* $[BMP4]_{max}$ *= 1.25 ng/ml, the upper threshold is not reported as it*
201 *coincides with the gradient window. Threshold for significance* $p<0.05$. *Dotted horizontal lines represent the mean of*
202 *lower and upper threshold concentrations of all replicates, occurring* 1.0±0.1 and 1.7 ±0.2 ng/ml *respectively*
203 *(mean*±s.e.m, n=12 independent experiments*).*

204 *Scale bars: 150µm.*

205

206

207

208 **An Endoderm tube sheathed with mesoderm cells emerges at the edge of BMP4 stimulated area.**

209 To dissect what happens at the edge of the stimulation window, we have developed a simplified variant of
210 the gradient chip, called µTransWells, creating patches of homogenously basally stimulated cells in an hESC
211 colony. Like the basal gradient chip, this device is fabricated by stamping PDMS on an anopore membrane
212 to block its pores everywhere except in 700µm-diameter disk-shaped windows, on top of which 4mm-
213 diameter PDMS wells are attached for individual stimulation, Fig.3AB. IF against pSMAD1 after 24 hours of
214 BMP4 stimulation confirmed that this device was able to produce a patch of homogeneous, BMP4
215 stimulated cells with a sharp boundary, Fig.3CD.

216 The device robustly reproduced the phenotype observed at the top edge of the gradient chip, *i.e.* after 72
217 hours, cells on the stimulation window were $[CDX2^+/ISL1^+/GATA3^+/TFAP2A^+]$ confirming the amnion-like
218 identity of cells receiving a high dose of BMP4 (10ng/ml), unstimulated cells remained $[SOX2^+/OCT4^+]$ and
219 in between emerged a thick domain with $TBXT^+$ and $SOX17^+$ cells, Fig.3EF,S3. Observation at higher
220 magnification revealed that this domain had a reproducible 3D structure with a hollow tube of $SOX17^+$ cells
221 surrounded by $TBXT^+$ cells. $SOX17^+$ cells co-expressed FOAX2, confirming their endoderm identity Fig.3GH,
222 movie 3.

223 $TBXT^+$ cells were detected on the stimulation window for lowered BMP4 concentrations between 0.6 to 2.5
224 ng/ml *i.e.* in a range comparable, although a bit wider, to the concentration thresholds in the gradient chip
225 (Figs.2, S3AB). However, unlike in the gradient chip, $TBXT^+$ cells were always observed as patches, in variable
226 amount, never covering more than 60% of the stimulation window, Fig.S3AB. By contrast, in WNT3a

227 stimulated µTransWells colonies, 100% of the cells on the stimulation window were TBXT$^+$. In that
228 condition, SOX17$^+$ cells also appeared at the frontier of stimulated and unstimulated domains but as
229 individual motile cells rather than as a close packed tube, figS3C, movie 4.

230

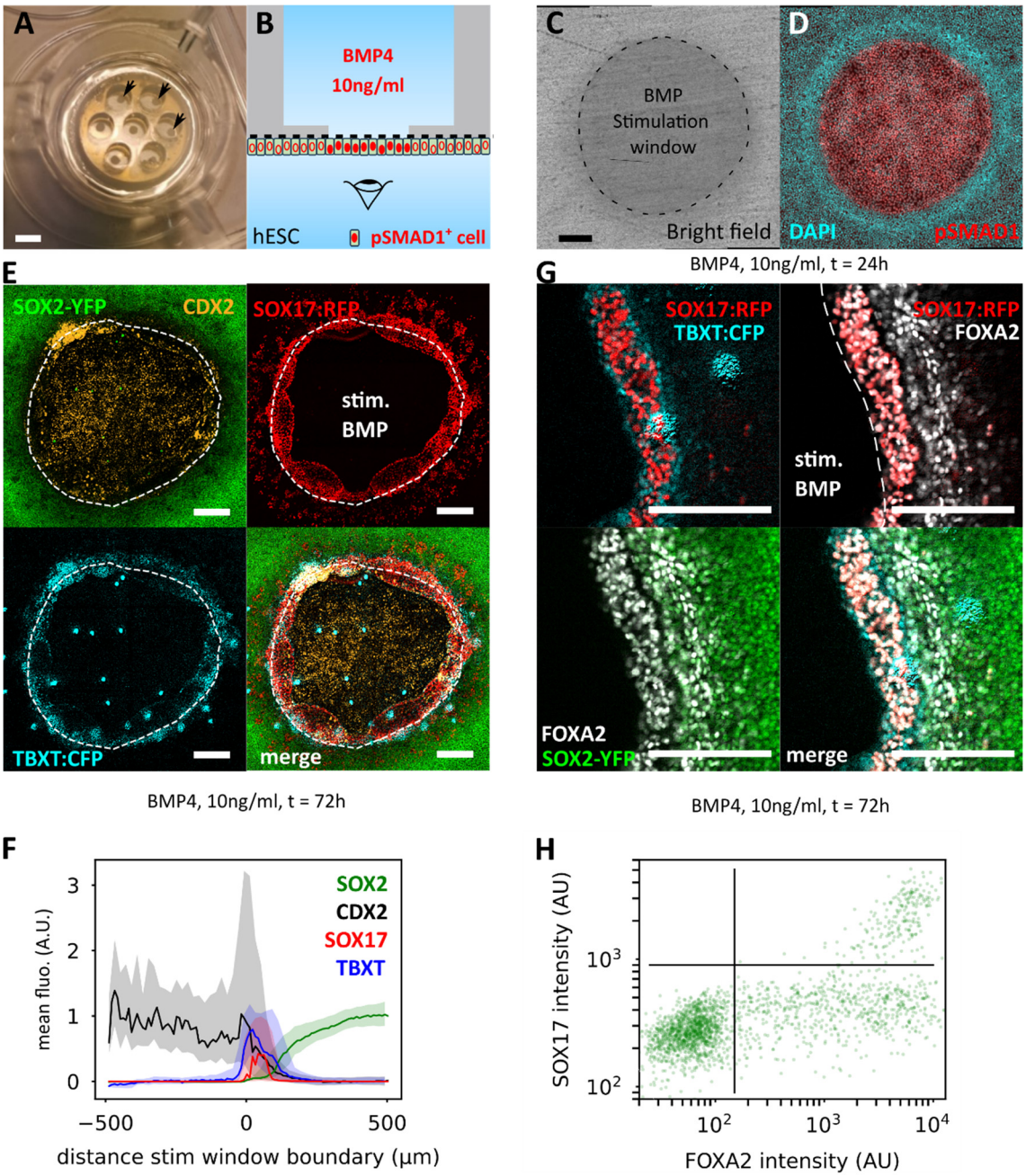

231

232 ***Figure 3. Production of well-defined signalling centers on hESC epithelia with the µTransWell device***

233 ***A)*** *Top view of a µTransWell device, with 4 mm-diameter small wells, each with a 700µm-diameter circular*
234 *stimulation patch (arrows). Scale bar 4mm.*

235 ***B)*** *Cross section of the culture system showing the experimental configuration. Cells are attached to one side of the*
236 *membrane in the bottom compartment and BMP4 is provided in the top compartment through the membrane but*
237 *only the cells in the area where the membrane is not blocked by PDMS receive the morphogen (pSMAD1 positive*
238 *cells, depicted with red-filled nuclei). Not to scale. Microscopy observation is achieved from the bottom.*

239 ***C,D)*** *Image of one µTransWell stimulation patch.* ***C)*** *Bright field. The darker-grey area is the non-obstructed part of*
240 *the membrane, where cells can receive BMP4.* ***D)*** *immunofluorescence against pSMAD1 after 24hours of BMP4*
241 *stimulation on the basal side of the central patch in the tissue. Scale bar 150µm.*

242 ***E)*** *Representative fluorescence images for the SOX2-YFP, TBXT:CFP and SOX17:RFP GLR reporter line, plus*
243 *immunofluorescence for CDX2 after 72h of stimulation of a central patch of the tissue with [BMP4] = 10ng/ml. Scale*
244 *bar 150µm.*

245 ***F)*** *Average fluorescence profiles after 72hours of BMP4 stimulation as a function of the distance to the edge of the*
246 *stimulation window. Colored areas represent the first and third quartile of individual cells from 3 independent*
247 *replicates.*

248 ***G)*** *Close-up view of the ring of differentiated cells at the edge of the BMP4 stimulation area* after 72hours of BMP4
249 stimulation *plus immunofluorescence for FOXA2. SOX17:RFP$^+$ cells co-express FOXA2 and are surrounded by*
250 *TBXT:CFP$^+$ cells. scale bar 150µm.*

251 **H)** *Quantification of FOXA2 and SOX17 co-expression after 72hours of BMP4 stimulation. Each dot represents a single*
252 *cell. All SOX17:RFP$^+$cells are also positive for FOXA2 (upper right quadrant).*

253

254 **Transient BMP4 stimulation triggers sustained WNT and NODAL signalling and permits endoderm**
255 **specification.**

256 We hypothesised that the emergence of TBXT$^+$ and SOX17$^+$ cells at the edge of the stimulation windows
257 was due to endogenous WNT and NODAL signalling as it has been reported in the embryo and in other *in*
258 *vitro* peri-gastrulation systems that BMP4 stimulation induces production of WNT3 and NODAL ligands[7,31,32].
259 Indeed, the band of TBXT$^+$ and SOX17$^+$ cells disappeared upon treatment with the WNT secretion inhibitor
260 IWP2, Fig.S3F.

261 We then investigated the spatio-temporal dynamics of activation of the BMP, NODAL and WNT signalling
262 pathways using IF and signalling reporter cell lines. As before, pSMAD1 stain was strictly restricted to the
263 stimulation area after 24 hours of BMP4 stimulation while cells positive for BRE:YFP, a transgenic reporter
264 of BMP activity[33] (Fig.1C&S4A), could be detected outside the stimulation area, Fig.4AB. The apparent
265 discrepancy between the BRE:YFP and pSMAD1 signals can easily be explained by their relative lifetime.
266 Indeed, inhibition of BMP signalling with LDN-193189 showed that pSMAD1 IF was back to baseline 30
267 minutes after inhibition while BRE:YFP was only reduced by 15% compared to control after 24 hours
268 (Fig.S4BC). This suggests that the BRE:YFP$^+$ cells outside the stimulation have received BMP4 in their past.
269 Time lapse imaging clearly showed that cells move outside the stimulation area, movie 5. Single cell tracking
270 experiment confirmed this hypothesis: 100% of tracks of BRE:YFP$^+$ cells found outside the stimulation
271 window after 24 hours of stimulation originated from the stimulation area, on which they had spent on
272 average 11+/-5 hours, Fig4.CD.

273 To record the activity of the WNT/β-catenin pathway with a higher temporal resolution than the BRE:YFP
274 system, we engineered a transgenic reporter cell line expressing a destabilized YFP (d2YFP) under the
275 control of the TCF/LEF synthetic reporter[34] (TCF/LEF:d2YFP). After 24hours of BMP4 stimulation,
276 TCF/LEF:d2YFP signal was elevated on the BMP4 stimulated area and spread about 50µm outside. By mixing
277 BRE:YFP and TCF/LEF:d2FFP cells in the same experiment (BRE:YFP cells having a Far Red nuclear marker to
278 distinguish them) we observed a strong correlation between the BRE and TCF spread at the single colony
279 level, Fig.S4J. ACTIVIN/NODAL pathway activity was assayed by IF against pSMAD2. It was also found to be

high on the stimulation window and spread further from its boundary than the BRE:YFP, TCF:d2YFP or TBXT signals (~70µm), Fig4FGH&S4.

At 48 hours, the ring of TBXT$^+$ cells was observed within the spread of BRE:YFP signal, showing that these cells have experienced BMP4 stimulation in their past, FigS4K-O. Taken together, these observations suggest that emergence of TBXT$^+$ cells outside the stimulation window results from sustained WNT and NODAL triggered by transient exposure to BMP4 and that WNT is the limiting factor for the differentiation of TBXT$^+$ cells. This condition permits the emergence of SOX17$^+$ definitive endoderm cells while the static gradient does not.

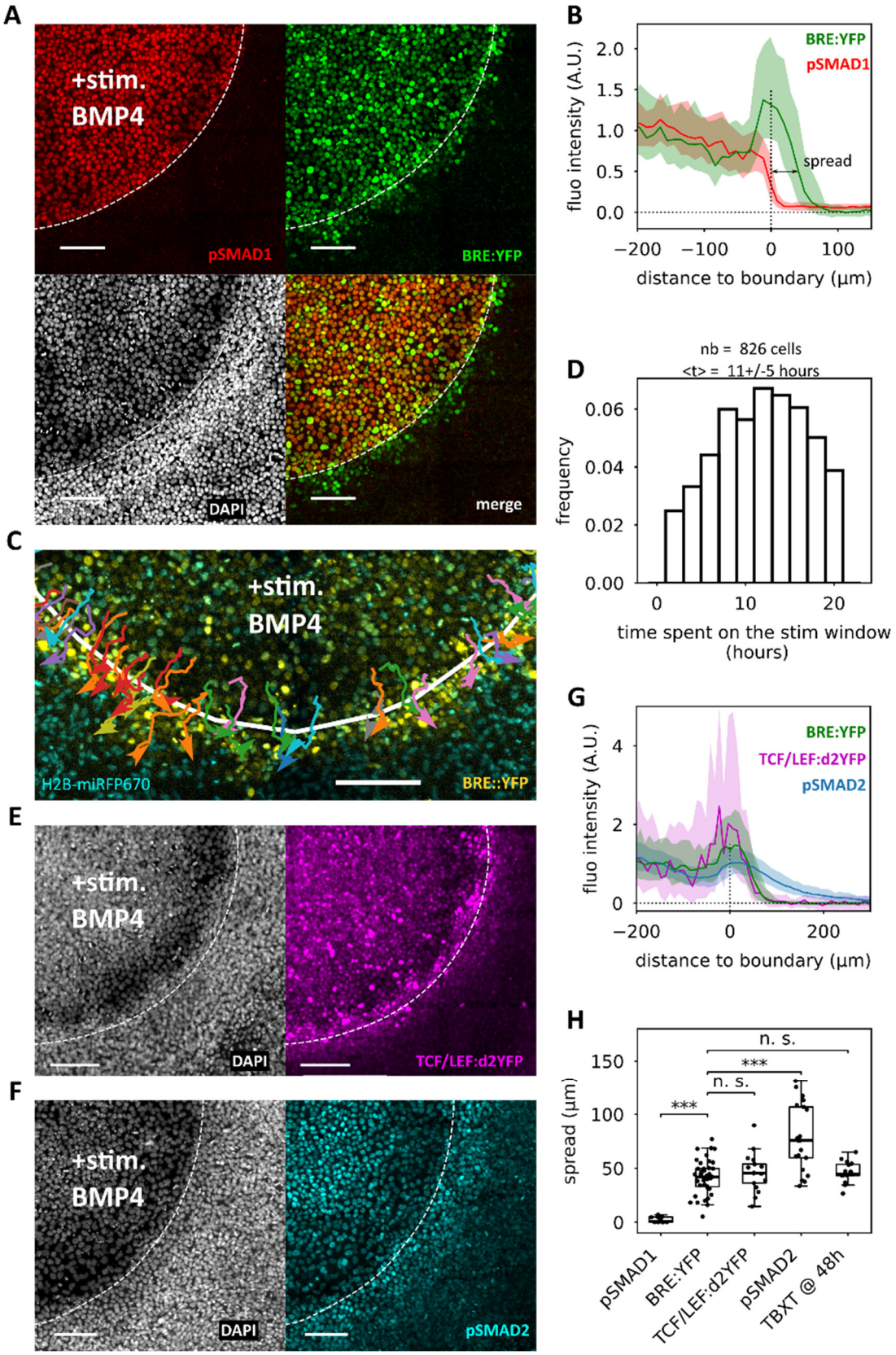

Figure 4: Differentiated cells outside the stimulation window have received a pulse of BMP4 that has activated WNT and NODAL signalling.

294 ***A)*** *Comparison of pSMAD1 immunofluorescence stain and BRE:YFP signal after 24 hours of stimulation of the central*
295 *patch of cells with BMP4 (10ng/ml). The white dotted line represents the boundary between stimulated and non-*
296 *stimulated regions of the tissue.*

297 ***B)*** *Average BRE:YFP and pSMAD1 fluorescence profiles after 24 hours of stimulation of the central patch of cells with*
298 *BMP4 (10ng/ml), as a function of the distance to the edge of the stimulation window. Fluorescence profiles are*
299 *normalized by the average of the signal within the stimulation window. Colored areas around the curves represent the*
300 *first and third quartile of individual cells. From these plots the spread of signalling is extracted, defined as the distance*
301 *at which the signalling curve becomes smaller than 0.5.*

302 ***C)*** *Single cell trajectories of BRE:YFP$^+$ cells and outside the stimulation window after 22hours of stimulation, showing*
303 *that all cells fitting both criteria have spent time in the stimulation window and thus have received BMP4.*

304 ***D)*** *Histogram of time spent on the stimulation window by BRE:YFP$^+$ cells positive and outside the stimulation window*
305 *22hours after the beginning of stimulation. N=826 cells from 12 colonies.*

306

307 ***E,F)*** *TCF/LEF:d2YFP (E) and pSMAD2 (F) Immunofluorescence stain after 24 hours stimulation of the central patch of*
308 *cells with BMP4 (10ng/ml).*

309 ***G)*** *Average BRE:YFP, TCF/LEF:d2YFP and pSMAD2 fluorescence profiles extracted from a single colony after 24 hours*
310 *of stimulation of the central patch of cells with BMP4 (10ng/ml), as a function of the distance to the edge of the*
311 *stimulation window. Colored areas represent the first and third quartile of individual cells from 3 independent*
312 *replicates.*

313 ***H)*** *Box plots representing the measured spread of signalling outside the stimulation area (as defined in B). Dots*
314 *represent individual replicates. Signalling reporters spread (pSMAD1, BRE:YFP, pSMAD2, TCF:d2YFP) have been*
315 *measured after 24 hours of BMP4 stimulation while position of the max of TBXT stain was assayed after 48 hours.*
316 *Threshold for significance: p-value of student's t-test <0.05.*

317 *Scale bars 100µm.*

318

319 **Patterning logic is well captured by a simple cell fate network with bistable WNT/NODAL signalling.**

320 We then asked if the logic of patterning observed could be consistent with the reported effect of BMP4
321 stimulation in the mouse embryo and in other peri-gastrulation *in vitro* systems[24]. We thus designed a
322 minimal Cell Fate Network incorporating the following interactions: BMP4 induces directly amnion-like
323 cells and the production of WNT and NODAL ligands[7,31,35] which promote induction of endoderm and
324 mesoderm cells[36]. Amnion-like and mesoderm identities cross-repress each other, and BMP4 prevents the
325 emergence of endoderm cells[28]. WNT and NODAL signalling self-activate[7,24,31,35]. The fact that TBXT is found
326 only in the area positive for both TCF/LEF:d2YFP and pSMAD2, suggests that WNT is limiting for
327 differentiation, therefore as a simplification, the model considers the 2 morphogens as a single entity
328 represented by WNT, Fig.5B and mathematical supplement. Considering their individual contribution would
329 be necessary, however, to resolve the fate choice between endoderm and mesoderm.

330 The mutual repression between Amnion-like and mesoderm identities was sufficient to obtain models
331 reproducing, after parameter optimisation, the emergence of 3 domains with boundary at constant
332 concentration thresholds in a static gradient of BMP4, Fig.5C, in a manner similar to the French Flag model[32],
333 with some significant differences, as described below. To recapitulate the presence of mesoderm and
334 endoderm cells outside the simulation window, the self-activation of WNT/NODAL was crucial to create a

335 bistable behaviour permitting the persistence of WNT and NODAL signalling after BMP stimulation had
336 stopped, Fig.5D, as further detailed in the Mathematical supplement.

337 The model should also account for the µTransWell experiment data as well as for the time development of
338 the patterns in static BMP4 gradients (Fig.S2). The differentiation dependence upon the duration of BMP4
339 stimulation in the µTransWell experiments determined the time scale of WNT dynamics to be about δ_W^{-1}
340 ~11 hours (Figs.4D, S4I&S5A). The WNT spatio-temporal dynamics is further constrained by the small extent
341 of the TXBT$^+$ region close to the high BMP4 end outside the gradient. This shows that the diffusion length
342 of WNT, $\ell_w=(\eta_w/\ \delta_W)^{1/2}$ should be smaller than 50µm and thus that WNT diffusion constant η_w should be
343 smaller than 0.06µm^2/s, in agreement with reported values in other settings[37].

344 The bistable behaviour of WNT dynamics, in combination with the parameter constraints, leads to two
345 important differences of our model with the French flag picture. Firstly, the low BMP4 boundary of the
346 TBXT$^+$ band is determined by the location of the front between high and low WNT concentrations rather
347 than directly by BMP4 concentration. Secondly, this WNT front moves at a slow speed. The above
348 constraints on WNT dynamics and diffusion were found compatible with the time development of the TBXT
349 fluorescence (Fig.S2) only if the TBXT$^+$ band after 72 hrs observed in our experiment (Fig.2) was still very
350 slowly growing at its low BMP4 boundary rather than fully stationary, as in the French flag picture. These
351 arguments are detailed further in the mathematical supplement.

352 To verify that WNT bistability was operating in our system, we performed inhibition experiments. We
353 observed that TCF/LEF signal persisted after inhibition of BMP signalling with a pharmalogical inhibitor,
354 Fig.S4GI. Inhibition of BMP or WNT signalling had also drastic consequence at the level of cell fate choice.
355 In µTransWells, the ring of TBXT$^+$ cells disappeared upon WNT signalling inhibition after 16 hours of BMP4
356 stimulation. This confirms that persistent WNT activity even when cells have moved outside the stimulation
357 area is necessary for mesoderm specification of those cells, Fig.5GH,S5BC. When BMP signalling was
358 inhibited after 16 or 24 hours of BMP4 stimulation, the amnion-like cells present on the stimulation area in
359 the control were mostly replaced by TBXT$^+$ cells. Sustained BMP4 stimulation is thus needed for amnion-
360 like cells specification which in turn prevents mesoderm, Figs.5E-H,S5A.

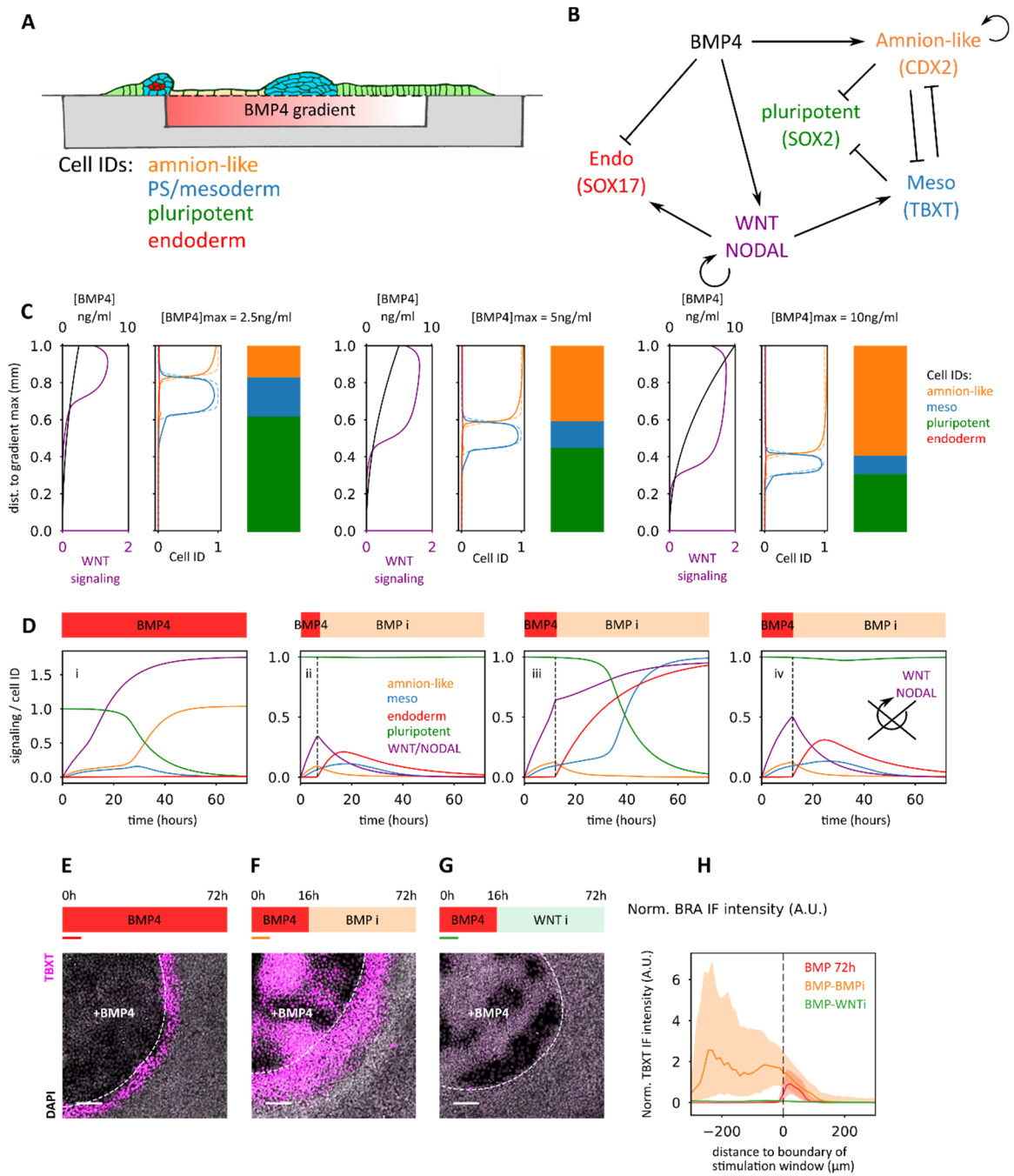

Figure 5: Model for patterning – Bistability of WNT

A) *Schematic summary of our observations. In the static gradient only 3 cell identities are observed. From minimum to maximum BMP4 concentration: undifferentiated, PS/mesoderm and amnion-like cells. Outside the stimulation area, at the edge between un-stimulated cells and those experiencing the high end of the gradient: mesoderm and endoderm are specified, dueto WNT and NODAL endogenous signalling triggered by transient BMP4 stimulation.*

B) *Proposed Cell Fate Network to explain the logic of patterning in our systems: BMP4 induces extra-embryonic amnion-like cell identity directly but also WNT and NODAL ligands that can induce mesoderm and endoderm fates. However, endoderm is blocked by BMP4. Amnion-like and PS/mesodermal fates cross inhibit. WNT and NODAL are secreted ligands so they can diffuse. WNT and Nodal self-activate. We have included the self-activation of amnion-like cells, which is found to be unimportant through parameter fitting.*

C) *Model prediction of patterning in a static gradient. For each* $[BMP4]_{max}$ *the left panel represents the applied BMP4 concentration gradient and the resulting WNT signalling profile, and the center panel represents the predicted cell fate*

patterning (solid lines). The right panel represents the expected pattern of cell identities based on experimental observations of figure 2, also denoted by sigmoidal profiles in the center panel (dashed lines).

D) *Model prediction of the outcome of transient BMP4 stimulation as experienced by cells in µTransWell experiments. (i) Cells staying on the stimulation window experience sustained BMP4 stimulation and amnion-like fate prevails. (ii) Transient but shorter than characteristic time to induce WNT self-activation results in no differentiation. (iii) At the edge of the stimulation window, cells experience transient BMP4 stimulation inducing self-sustained WNT signalling and PS/mesoderm identity. (iv) Without WNT self-activation, transient stimulation does not induce differentiation.*

E,F,G) *TBXT stains on a µTransWell after 72h BMP4 (CTRL), 16h BMP4 followed by 56h BMP inhibition (BMPi) and 16h BMP4 followed by 56h WNT inhibition (WNTi). After BMPi, TBXT is everywhere showing that sustained BMP4 is needed to get the amnion-like fate. WNTi leads to no TBXT+ cells, indicating that this fate needs sustained WNT activity and therefore that bistable WNT is necessary. Scale bars 100µm.*

H) *Average fluorescence profiles for the 3 conditions described in panels EFG for n = (13, 13, 15) colonies respectively, from 3 independent experiments. Colored areas represent the spread between the 1st and 3rd quartiles of the distribution of individual cells. Profiles are normalized to the maximum of the average TBXT profile in the BMP72h condition.*

391 **Discussion**

392 BMP has been shown to work as a morphogen, *i.e.* controlling cell fate in a dose dependent manner, in a
393 variety of developmental contexts[16]. The situation is less clear for *in vitro* hESC directed
394 differentiation[20,26,38]. Isolated or low-density hESCs can only differentiate in amnion like cells if stimulated
395 with a high enough dose of BMP4 while in denser 2D cultures, mesoderm cells can appear in an
396 intermediate range of BMP4 concentration, but never as a pure population[39]. Finally, cells from the three
397 germ layers are generated in BMP4 stimulated micropatterned hESC colonies[30]. Together, these
398 observations lead to the conclusion that hESCs could not reliably interpret concentration as a predictive
399 differentiation cue[24].

400 Here we introduce microfluidic devices that, taking inspiration from where the BMP4 molecules are
401 delivered to the mouse epiblast, allow stimulating epithelial tissues on their basal side with defined spatio-
402 temporal profiles of morphogen. In static parabolic gradients of BMP4, hESCs differentiate into a sharp and
403 reproducible pattern of 3 cell identities with a central band containing 100% of $TBXT^+$ mesoderm cells. The
404 two cell fate thresholds happen at constant concentrations, in the dynamic range of the sensitivity of the
405 BMP pathway, thus establishing that absolute concentration of BMP4 can provide positional information
406 for hESCs to solve Wolpert's French Flag problem[40,41]. Basal stimulation with a spatial gradient, however, is
407 necessary to reveal the morphogen effect as the BMP induced mesoderm domain is not stable over large
408 areas as shown in µTransWells dose response experiments.

409 Under static gradient conditions however, cells have access to only 2 differentiated identities, amnion-like
410 and extra-embryonic mesoderm. Unlike in h2D-gastruloids[4,30], other embryonic derivatives of the PS such
411 as definitive endoderm are absent. Gastrulation is a dynamic process during which cells are certainly
412 experiencing dynamic stimulation. Our observation of cell differentiation at the edge between stimulated
413 and unstimulated regions of tissues illustrates possible consequences. Using live reporter of signalling and
414 tracking of cell position, we established that this differentiation was due to cell moving away from the BMP
415 stimulation area, thus experiencing a transient exposure to BMP. Inhibition experiments and modelling
416 further showed that, in line with a recent report[24], the key regulatory network feature to explain this effect
417 is the bistable expression of secondary morphogens WNT and NODAL.

418 Thus, besides generating a temporal morphogen effect, modulating the duration of BMP exposure also
419 increased the repertoire of accessible fates, as endoderm cells emerged among those cells transiently
420 exposed to BMP. Prolonged exposure to BMP does not induce endoderm *in vitro*[42] as this prevents its
421 emergence[28,29]. Short stimulation, however, has been used to induce posterior foregut organoids[43].
422 Generation of endoderm after a short pulse of BMP is consistent with fate mapping experiments in the
423 gastrulating mouse embryo reporting that endoderm cells can emerge from rather proximal regions of the
424 PS[44]. These cells could experience transient exposure to BMP by migrating away from the source and
425 expressing BMP inhibitors such as CER1. Effectively transient exposure to BMP could also explain the
426 emergence of endoderm cells in BMP stimulated hESC micropatterned colonies[4,30].

427 Thus, our basal stimulation devices circumvent a major source of variability in interpretation of BMP
428 concentration, namely the loss of accessibility to receptors of apically provided ligands due to gradual
429 segregation of receptors on the basal side during maturation of the epithelium. They allowed us, combined
430 with live reporters of signalling and cell fates, to establish the causality link between the morphogen
431 landscape experienced by the tissue and the resulting patterning. As morphogen gradients and morphogen-
432 induced signalling centres are ubiquitous in development[45], and given that in a number of situations such

as neural tube patterning, morphogens are provided on the basal side of epithelia, we expect our experimental strategy to be widely applicable to dissect the mechanism of patterning of other developing organs and for precise tissue engineering.

####### end of main text ################

Methods

Design of microfluidic device. among the many gradient-making devices available in the microfluidics toolbox (reviewed in[46]) we have favoured a design using successive mixing as it allows for more flexibility in the gradient shape and temporal variation of the gradient. We have thus adapted an original design of Jeon *et al.* [11] according to estimated diffusive properties of BMP4. Previous measurements of the diffusion coefficient of freely diffusing BMP and other proteins of comparable molecular weights give an order of magnitude estimate for a diffusion coefficient of $D_B \approx 50\ \mu m^2 s^{-1}$ [47,48]. This diffusion coefficient constrains the device design due to the requirement that complete mixing by diffusion must occur in each serpentine channel. We thus chose channel dimensions and a flow rate which satisfy the condition that the root-mean-squared distance travelled by BMP4 during passage in a single serpentine channel is greater than half the channel width. That is, that

$$d_{rms} = \sqrt{2D_B t} > \frac{w_s}{2}$$

where t is the passage time for liquid travelling through a serpentine channel and w_s is the width of the serpentine channel. Dimensions of $70\ \mu m * 8300\ \mu m * 150\ \mu m$ (width $*$ length $*$ height) and a flow rate (for each of the three inlet channels) of $10\ \mu L.s^{-1}$ were thus chosen to satisfy this condition. The chosen flow rate, within the stimulation chamber of dimensions $1000\ \mu m * 4000\ \mu m * 150\ \mu m$ (width $*$ length $*$ height) results in an estimated root-mean-squared displacement of $\sim 85\ \mu m$ for BMP during passage through the stimulation chamber. We expect only minimal change in the profile of the gradient from inlet to outlet, since this is small compared with the chamber width.

Manufacture of PDMS microfluidic chips. The microfluidic design was drawn in vector graphics software Inkscape and imaged onto polyester film with a photographic emulsion coating to create a mask (JD Photo Data). The resin mould for casting the microfluidic chip was created using standard protocols from photolithography. Briefly, SU8 photoresist **(microresist,GmBH)** was spun onto a Si wafer to a thickness of 150 µm and then baked for 1hr at 95°C. The mask was put in contact with the baked resin and exposed to UV for 60 s. This was then baked again for 1hr at 95°C before developing in SU8 developer for 20 min. The mould was then silanized for 1 hr under vacuum using (3-Mercaptopropyl)trimethoxysilane (Sigma). The PDMS microfluidic chip was carefully cut out of the mould using a scalpel and holes were punched in the inlets and outlets.

Patterned stamp-and-stick to bond the chip to the membrane. Basal delivery of BMP4 to hESC colonies imposes to bind the microfluidic chip to a porous membrane. This is a common feature of organ on chip devices, however in most cases they incorporate PDMS or track-etch membranes with low pore density (10^6 pores / cm^2, i.e ~1 pore./cell on average) which we found were not suitable for our application as BMP stimulation though these membranes resulted in a spatially heterogenous response. We thus used anopore membranes (Whatman anodisc, 0.2µm pores) which have around 80% porosity. As common bonding techniques such as plasma bonding do not work to robustly bond the microfluidic chip to anopre membrane, we combined the stamp-and-stick [49,50] and multilayer soft lithography[14] techniques. Briefly, a thin layer of PDMS was stamped onto the membrane using a custom-made PDMS stamp. The stamp was made by casting PDMS from an SU-8 mould consisting of a single raised rectangle which matched the dimensions of the stimulation window of the gradient chip. Thus, the resulting stamp deposited PDMS onto the membrane everywhere apart from the stimulation window. To ink the stamp, a thin layer of PDMS was spun onto a glass coverslip and the stamp was placed face-down onto the coated glass. The stamp was removed and left in a dust-free environment for 10 minutes to allow inhomogeneities in the PDMS thickness

479 to relax. The stamp was then carefully placed on the membrane, left for 30 seconds to ensure uniform
480 contact, and then carefully removed. The microfluidic chip was aligned by hand under a magnifying glass
481 and pressed against the membrane and backed at 65°C for 1 hr. The stamping of PMDS thus served the
482 dual-purpose of bonding the chip to the membrane and blocking membrane pores in all regions where
483 apical to basal communication should not occur, see Fig S1.

484 **Microfluidic experiment preparation.** PTFE tubing was rinsed with deionised water and then autoclaved.
485 GasTight glass syringes (Hamilton; 0.5 mL) and pressure vials were sterilised in a 70% ethanol bath followed
486 by rinsing in deionised water. The tubing and syringes were filled with the required stimulation media and
487 connected, taking care not to trap bubbles. The microfluidic device was the treated for 7 min with deep UV
488 (Jelight UVO cleaner) and a 70 µL droplet of Laminin-521 (Stemcell Technologies), diluted in PBS+/+ (Sigma)
489 to 20 µg mL^{-1}, was placed on the membrane, covering the stimulation window, for 45 min, see Fig.S1.

490 **hPSC cell lines, culture and differentiation.** The RUES2 and RUES2 GLR hESC cell lines were kindly provided
491 by A. H. Brivanlou (Rockefeller University, NY, USA). All experiments were declared to the French Agence
492 de la Biomedecine, authorisation number RE16-004RCI and RE21-001RC. hESC were cultured on culture
493 dishes coated in Geltrex (Thermo Fisher Scientific) in mTeSR according to the manufacturer's guidelines.
494 iPSC029 cell line is a kind gift of Mickael Kyba (University of Minnesota, USA). Cultures were tested for
495 mycoplasma infection once a month. Gradient chip experiments were performed with the RUES2 parental
496 line and the GLR and signalling reporter subclones. µTransWell experiments were performed with the
497 various RUES2 subclones and the iPSC0029 cell line with similar outcome. hESC and hiPSC were cultivated
498 in mTeSR plus medium according to manufacturer's instruction on tissue culture dishes coated with
499 1%Geltrex solutions. Prior to seeding on microfluidic devices, hESC were harvested as a single cell
500 suspension using accutase (sigma) incubated for 6 minutes at 37°C a drop of cell suspension (2-3.5.10^6
501 cells/ml) in mTeSR medium supplemented with ROCK inhibitor (RI,20µM) was positioned on top of
502 stimulation window of the devices and cells were allowed to attach to the substrate for 45 minutes. The
503 devices were then transferred in the imaging cuvette filled with mTeSR+RI for 45 additional minutes after
504 which the medium was replaced by mTeSR. Stimulation started between 4 to 15 hours after seeding with
505 BMP4 [R&D System, 314-BP], WNT3A [R&D System, 5036-WN] at concentration specified in each
506 experiment. Pharmacological agonists or inhibitors were used at the following concentration unless
507 otherwise specified: CHIR99021 [3µM, cell guidance systems, SM13], LDN193189 [100nM Cell Guidance
508 System SM23], IWP2 [2µM, Stemcell Technologies, 72122], SB431542 [20µM, cell guidance systems, SM33],
509 XAV939[5µM, cell guidance systems, SM38]

510 **Reporter cell lines** the RUES2 GLR cell line generation and validation has been described in [18]. It is
511 engineered to report for the expression of three independent fate reporters: SOX2–mCitrine (SOX2-YFP),
512 BRA–2A-mCerulean (TBXT:CFP) and SOX17-2A–tdTomato (SOX17:RFP). Fluorescent reporter proteins were
513 inserted at the endogenous loci using crispr/cas9 gene editing. The BRE:YFP and TCF/LEF:d2YFP clonal and
514 stable transgenic RUES2 lines were generated using the ePiggyBAC transposable elements system [51]. the
515 BRE element (addgene plasmid#45126, [33]) was cloned in a ePiggyBAC plasmid containing a puromycin
516 resistance cassette vector (gift of AH Brivanlou) upstream of a minP minimal promoter (from Promega
517 pGL4) and a YFP. The TCF/LEF (addgene #32610 [34]) was cloned upstream of a hsp68 minimal promoter and
518 d2YFP, a destabilized version of YFP with a lifetime of 2h. Cells were transfected using lipofectamine 3000
519 following manufacturer's instruction. Selection with puromycin (0.5µg/ml) was started 48h after
520 transfection. After a week of selection cells were seeded at clonal density (100-200 cells in a 35mm dish) in

521 mTeSR supplemented with CloneR2 (stemcells technologies). Clones were picked manually and assayed for
522 their capacity to respond to BMP4 or CHIR treatment.

523 **Immunofluorescence.** Tissues attached to membranes were fixed by placing the transwell in a 6-well dish
524 containing in 4% PFA for 25 min and were then washed 3 times for 15 min in PBS. They were then blocked
525 and permeabilised in 2% bovine serum albumin with 1% triton-100 (Sigma) for 30 min. The tissue was
526 washed again in PBS incubated with primary antibody in blocking solution overnight at 4°C. The tissue was
527 then washed 3 times for 30 min in PBS before incubating with the secondary antibody for 2 hr at room
528 temperature. The tissue was then washed in PBS and kept in PBS at 4°C until imaging. See table below for
529 a list of used antibodies.

530 **Imaging.** All imaging was performed on an inverted Olympus IX83 equipped with DSD2 confocal module
531 (Andor). Montage scans were performed using a motorised stage (Märzhäuser). Sample was maintained at
532 37°C and 5%CO2.

533 **Image analysis.** Image processing was performed using custom-made routines. Fluorescence illuminations
534 inhomogeneities were corrected using the BaSIC algorithm[52], tiles were assembled using the grid/collection
535 stitching Fiji pluggin[53]. Nuclei segmentation was performed with stardist [54] and tracking with trackmate [55]

536 **Mathematical modelling.** The cell fate network model (Fig.5B) is described by the following
537 nondimensional differential equations

538 $$B = \frac{b^{n_b}}{k_b^{n_b} + b^{n_b}}, \tag{1}$$

539 $$\frac{1}{d_w}\frac{\partial W}{\partial t} = D_w \frac{\partial^2 W}{\partial y^2} + \frac{a_w B^{n_w}}{k_w^{n_w} + B^{n_w}} + \frac{W^{\bar{n}_w}}{\bar{k}_w{}^{\bar{n}_w} + W^{\bar{n}_w}} - W, \tag{2}$$

540 $$\frac{1}{d_x}\frac{dX}{dt} = \left(\frac{B^{n_x}}{k_x^{n_x} + B^{n_x}} + \frac{\bar{a}_x X^{\bar{n}_x}}{\bar{k}_x^{\bar{n}_x} + X^{\bar{n}_x}}\right)\frac{1}{(1 + (M/l_x)^{r_x})\left(1 + \left(P/l_{xp}\right)^{r_{xp}}\right)} - X, \tag{3}$$

541 $$\frac{1}{d_m}\frac{dM}{dt} = \frac{W^{n_m}}{\left(k_m^{n_m} + W^{n_m}\right)(1 + (X/l_m)^{r_m})\left(1 + \left(P/l_{mp}\right)^{r_{mp}}\right)} - M, \tag{4}$$

542 $$\frac{1}{d_e}\frac{dE}{dt} = \frac{W^{n_e}}{\left(k_e^{n_e} + W^{n_e}\right)(1 + (B/l_e)^{r_e})} - E, \tag{5}$$

543 $$\frac{1}{d_p}\frac{dP}{dt} = \frac{(1 + k_p)P}{(k_p + P)\left(1 + \left(X/l_{px}\right)^{r_{px}}\right)\left(1 + \left(M/l_{pm}\right)^{r_{pm}}\right)} - P. \tag{6}$$

544 Eq. (1) describes the activation of the BMP4 signalling pathway as a Hill function, which can be
545 interpreted as a generalised Michaelis-Menton kinetics. Eq. (2) describes the diffusion, activation by
546 BMP4 response, and self-activation of WNT/NODAL. We have used the concentration of WNT to
547 represent the overall activation level of the WNT/NODAL pathway, as justified in the main text and the
548 supplementary mathematical information (SM) . Eqs. (3-5) govern the evolution of cell fate likelihoods for
549 the three different cell types that we consider: amnion-like (*X*), mesoderm (*M*), and endodermal (*E*). Eq.
550 (6) describes the baseline pluripotent cell state. Eqn. (2) takes into account WNT/NODAL diffusion within
551 the tissue which plays an important role in the gradient chip. Given a known spatio-temporal BMP4
552 stimulation profile, we simulated the evolution of cell fates in an experimental scenario (gradient chip or

μTransWell) by solving the equations numerically using the forward Euler scheme and the standard central finite difference to discretise the spatial derivative of *W*.

The parameters in Eq. (1-6) are provided in table M3 in the SM. The parameters $n_b, k_b, n_w, k_w, \bar{n}_w, \bar{k}_w, a_w, d_w, D_w$, were obtained from our experimental measurements and data in the previous literature. We fitted the other model parameters $\mathbf{p} = [n_x, k_x, r_x, l_x, \bar{n}_x, \bar{k}_x, \bar{a}_x, d_x, n_m, k_m, r_m, l_m, d_m]$ against imaging data of cell fate distributions from the microfluidic gradient chip at different BMP4 stimulation strengths. The fitting was based on minimising a cost function measuring the difference between the model predicted and experimentally imaged cell fate profiles at the given time t_g when measurement was taken:

$$f(\mathbf{p}) = \begin{cases} 10, & \text{if } k_x < 0, \bar{k}_x < 0, k_m < 0, l_x < 0, \text{ or } l_m < 0, \\ \sum_{j=1}^{3} \left[\int_0^1 \left(X_j(y, t_g) - \hat{X}_j(y) \right)^2 + \left(M_j(y, t_g) - \hat{M}_j(y) \right)^2 dy \right], & \text{otherwise.} \end{cases}$$

$\hat{X}_j(y), \hat{M}_j(y)$ are experimentally identified target cell identity marker distributions, and the subscript j ($j = 1,2,3$) denotes three different gradient maximums. To solve the optimisation problem, we adopted the Nelder-Mead method. All numerical calculations were performed with in-house codes written in Julia utilising open-source packages. More details of modelling and extended discussions about our results can be found in the SM. Parameters that are used to produce Fig.5CD are reported in Table M3 in the supplementary. Numerical codes for simulations and analyses are available in the publicly available Github repository (see **Data availability**).

Data availability:

Sample experimental images, Matlab and Python codes to process and analyze the images, and Julia codes for model simulations and analyses are available in the repository:
https://github.com/bsorre/wyatt_gradients

578 **table of primary antibodies used for this study**

Antibody	Organism	Dilution	Supplier	Reference
SOX2	Rat	1:500	invitrogen	14-9811-82
OCT3/4	Mouse	1:300	BD Biosciences	611203
Brachyury/TBXT	Goat	1:300	R&D Systems	AF2085
SOX17	Goat	1:300	R&D Systems	AF1924
FOXA2	Rabbit	1:250	Cell Signalling	8186S
pSMAD1/5	Rabbit	1:250	Cell Signalling	13820
LEF1	Rabbit	1:250	Cell Signalling	2230S
pSMAD2/3	Rabbit	1:250	Cell Signalling	18338
CDX2	Mouse	1:250	Abcam	ab157524
CDX2	Rabbit	1:300	Abcam	ab76541
ISL1	Mouse	1:50	DSHB	39.4D5-c
GATA3	Goat	1:300	R&D systems	AF2605
TFAP2A	Mouse	1:50	santa cruz biotechnologies	sc-12726

579

secondary: donkey anti:				
target species	**fluorophore**	**supplier**	**ref**	**dilution**
Mouse	Alexa488	Abcam	ab150109	1:500
Rat	DyLight488	Thermofischer	SA5-10026	1:500
Rabbit	Alexa555	Abcam	ab150062	1:500
Goat	Alexa555	Abcam	ab150134	1:500
Mouse	Alexa647	Abcam	ab150111	1:500
Goat	Alexa647	Abcam	ab150135	1:500
Rabbit	Alexa647	Abcam	ab150063	1:500

580

581 **References**

582 1. Bardot, E. S. & Hadjantonakis, A.-K. Mouse gastrulation: Coordination of tissue patterning,
583 specification and diversification of cell fate. *Mech. Dev.* **163**, 103617 (2020).
584 2. Camacho-Aguilar, E. & Warmflash, A. Insights into mammalian morphogen dynamics from embryonic
585 stem cell systems. in *Current Topics in Developmental Biology* vol. 137 279–305 (Elsevier, 2020).
586 3. Morgani, S. M. & Hadjantonakis, A.-K. Signaling regulation during gastrulation: Insights from mouse
587 embryos and in vitro systems. in *Current Topics in Developmental Biology* vol. 137 391–431 (Elsevier,
588 2020).
589 4. Warmflash, A., Sorre, B., Etoc, F., Siggia, E. D. & Brivanlou, A. H. A method to recapitulate early
590 embryonic spatial patterning in human embryonic stem cells. *Nat. Methods* **11**, 847–854 (2014).
591 5. Tewary, M. *et al.* A stepwise model of reaction-diffusion and positional information governs self-
592 organized human peri-gastrulation-like patterning. *Development* **144**, 4298–4312 (2017).
593 6. Heemskerk, I. *et al.* Rapid changes in morphogen concentration control self-organized patterning in
594 human embryonic stem cells. *eLife* **8**, e40526 (2019).
595 7. Chhabra, S., Liu, L., Goh, R., Kong, X. & Warmflash, A. Dissecting the dynamics of signaling events in
596 the BMP, WNT, and NODAL cascade during self-organized fate patterning in human gastruloids. *PLOS*
597 *Biol.* **17**, e3000498 (2019).
598 8. Manfrin, A. *et al.* Engineered signaling centers for the spatially controlled patterning of human
599 pluripotent stem cells. *Nat. Methods* **16**, 640–648 (2019).
600 9. Zhang, Z., Zwick, S., Loew, E., Grimley, J. S. & Ramanathan, S. Mouse embryo geometry drives
601 formation of robust signaling gradients through receptor localization. *Nat. Commun.* **10**, 1–14 (2019).
602 10. Etoc, F. *et al.* A Balance between Secreted Inhibitors and Edge Sensing Controls Gastruloid Self-
603 Organization. *Dev. Cell* **39**, 302–315 (2016).
604 11. Jeon, N. L. *et al.* Generation of Solution and Surface Gradients Using Microfluidic Systems. *Langmuir*
605 **16**, 8311–8316 (2000).

606 12. Cheng, J. W. *et al.* “Chip-on-a-Transwell” Devices for User-Friendly Control of the Microenvironment
607 of Cultured Cells. *ACS Appl. Bio Mater.* **2**, 4998–5011 (2019).
608 13. Corral-Nájera, K., Chauhan, G., Serna-Saldívar, S. O., Martínez-Chapa, S. O. & Aeinehvand, M. M.
609 Polymeric and biological membranes for organ-on-a-chip devices. *Microsyst. Nanoeng.* **9**, 1–25
610 (2023).
611 14. Unger, M. A., Chou, H.-P., Thorsen, T., Scherer, A. & Quake, S. R. Monolithic Microfabricated Valves
612 and Pumps by Multilayer Soft Lithography. *Science* **288**, 113–116 (2000).
613 15. Evenou, F., Di Meglio, J.-M., Ladoux, B. & Hersen, P. Micro-patterned porous substrates for cell-based
614 assays. *Lab. Chip* **12**, 1717 (2012).
615 16. Akiyama, T., Raftery, L. A. & Wharton, K. A. Bone morphogenetic protein signaling: the pathway and
616 its regulation. *Genetics* **226**, iyad200 (2024).
617 17. Peng, G. *et al.* Spatial Transcriptome for the Molecular Annotation of Lineage Fates and Cell Identity
618 in Mid-gastrula Mouse Embryo. *Dev. Cell* **36**, 681–697 (2016).
619 18. Martyn, I., Kanno, T. Y., Ruzo, A., Siggia, E. D. & Brivanlou, A. H. Self-organization of a human
620 organizer by combined Wnt and Nodal signalling. *Nature* **558**, 132–135 (2018).
621 19. Shao, Y. *et al.* Self-organized amniogenesis by human pluripotent stem cells in a biomimetic
622 implantation-like niche. *Nat. Mater.* **16**, 419–425 (2017).
623 20. Zheng, Y. *et al.* Controlled modelling of human epiblast and amnion development using stem cells.
624 *Nature* **573**, 421–425 (2019).
625 21. Yang, R. *et al.* Amnion signals are essential for mesoderm formation in primates. *Nat. Commun.* **12**,
626 5126 (2021).
627 22. Chhabra, S. & Warmflash, A. BMP-treated human embryonic stem cells transcriptionally resemble
628 amnion cells in the monkey embryo. *Biol. Open* **10**, bio058617 (2021).
629 23. Ohgushi, M., Taniyama, N., Vandenbon, A. & Eiraku, M. Delamination of trophoblast-like syncytia
630 from the amniotic ectodermal analogue in human primed embryonic stem cell-based differentiation
631 model. *Cell Rep.* **39**, (2022).

632 24. Camacho-Aguilar, E. *et al.* Combinatorial interpretation of BMP and WNT controls the decision
633 between primitive streak and extraembryonic fates. *Cell Syst.* **0**, (2024).
634 25. Morgani, S. M., Metzger, J. J., Nichols, J., Siggia, E. D. & Hadjantonakis, A.-K. Micropattern
635 differentiation of mouse pluripotent stem cells recapitulates embryo regionalized cell fate patterning.
636 *eLife* **7**, e32839 (2018).
637 26. Bernardo, A. S. *et al.* BRACHYURY and CDX2 Mediate BMP-Induced Differentiation of Human and
638 Mouse Pluripotent Stem Cells into Embryonic and Extraembryonic Lineages. *Cell Stem Cell* **9**, 144–155
639 (2011).
640 27. Pijuan-Sala, B. *et al.* A single-cell molecular map of mouse gastrulation and early organogenesis.
641 *Nature* **566**, 490–495 (2019).
642 28. Plouhinec, J.-L., Simon, G., Vieira, M., Collignon, J. & Sorre, B. Dissecting signaling hierarchies in the
643 patterning of the mouse primitive streak using micropatterned EpiLC colonies. *Stem Cell Rep.*
644 https://doi.org/10.1016/j.stemcr.2022.05.009 (2022) doi:10.1016/j.stemcr.2022.05.009.
645 29. Simon, G., Plouhinec, J.-L., Gilardi-Hebenstreit, P., Sorre, B. & Collignon, J. BMP signaling modulations
646 control primitive streak patterning. 2024.10.01.616050 Preprint at
647 https://doi.org/10.1101/2024.10.01.616050 (2024).
648 30. Minn, K. T. *et al.* High-resolution transcriptional and morphogenetic profiling of cells from
649 micropatterned human ESC gastruloid cultures. *eLife* **9**, e59445 (2020).
650 31. Ben-Haim, N. *et al.* The Nodal Precursor Acting via Activin Receptors Induces Mesoderm by
651 Maintaining a Source of Its Convertases and BMP4. *Dev. Cell* **11**, 313–323 (2006).
652 32. Tortelote, G. G. *et al.* Wnt3 function in the epiblast is required for the maintenance but not the
653 initiation of gastrulation in mice. *Dev. Biol.* **374**, 164–173 (2013).
654 33. Korchynskyi, O. & Dijke, P. ten. Identification and Functional Characterization of Distinct Critically
655 Important Bone Morphogenetic Protein-specific Response Elements in the Id1 Promoter *. *J. Biol.*
656 *Chem.* **277**, 4883–4891 (2002).

657 34. Ferrer-Vaquer, A. *et al.* A sensitive and bright single-cell resolution live imaging reporter of Wnt/ß-
658 catenin signaling in the mouse. *BMC Dev. Biol.* **10**, 121 (2010).
659 35. Tortelote, G. G. *et al.* Wnt3 function in the epiblast is required for the maintenance but not the
660 initiation of gastrulation in mice. *Dev. Biol.* **374**, 164–173 (2013).
661 36. Wang, L. & Chen, Y.-G. Signaling Control of Differentiation of Embryonic Stem Cells toward
662 Mesendoderm. *J. Mol. Biol.* **428**, 1409–1422 (2016).
663 37. Mii, Y. *et al.* Quantitative analyses reveal extracellular dynamics of Wnt ligands in Xenopus embryos.
664 *eLife* **10**, e55108 (2021).
665 38. Roberts, R. M. *et al.* Differentiation of trophoblast cells from human embryonic stem cells: to be or
666 not to be? https://doi.org/10.1530/REP-14-0080 (2014) doi:10.1530/REP-14-0080.
667 39. Nemashkalo, A., Ruzo, A., Heemskerk, I. & Warmflash, A. Morphogen and community effects
668 determine cell fates in response to BMP4 signaling in human embryonic stem cells. *Development* **144**,
669 3042–3053 (2017).
670 40. Wolpert, L. Positional Information and the Spatial Pattern of Cellular Differentiationt. *J Theor. Biol* **25**,
671 1–47 (1969).
672 41. Sharpe, J. Wolpert's French Flag: what's the problem? *Development* **146**, dev185967 (2019).
673 42. D'Amour, K. A. *et al.* Efficient differentiation of human embryonic stem cells to definitive endoderm.
674 *Nat. Biotechnol.* **23**, 1534–1541 (2005).
675 43. Lin, F. *et al.* Mechanically enhanced biogenesis of gut spheroids with instability-driven
676 morphomechanics. *Nat. Commun.* **14**, 6016 (2023).
677 44. Kinder, S. J. *et al.* The orderly allocation of mesodermal cells to the extraembryonic structures and the
678 anteroposterior axis during gastrulation of the mouse embryo. *Development* **126**, 4691–4701 (1999).
679 45. Anderson, C. & Stern, C. D. Chapter Twenty-Six - Organizers in Development. in *Current Topics in*
680 *Developmental Biology* (ed. Wassarman, P. M.) vol. 117 435–454 (Academic Press, 2016).
681 46. Wu, Z. *et al.* A review on the development and application of microfluidic concentration gradient
682 generators. *Phys. Fluids* **36**, 072014 (2024).

683 47. Davis, H., Raja, E., Miyazono, K., Tsubakihara, Y. & Moustakas, A. Mechanisms of action of bone
684 morphogenetic proteins in cancer. *Cytokine Growth Factor Rev.* **27**, 81–92 (2016).
685 48. Pomreinke, A. P. *et al.* Dynamics of BMP signaling and distribution during zebrafish dorsal-ventral
686 patterning. *eLife* **6**, e25861 (2017).
687 49. Satyanarayana, S., Karnik, R. N. & Majumdar, A. Stamp-and-stick room-temperature bonding
688 technique for microdevices. *J. Microelectromechanical Syst.* **14**, 392–399 (2005).
689 50. Evenou, F., Di Meglio, J.-M., Ladoux, B. & Hersen, P. Micro-patterned porous substrates for cell-based
690 assays. *Lab. Chip* **12**, 1717–1722 (2012).
691 51. Lacoste, A., Berenshteyn, F. & Brivanlou, A. H. An efficient and reversible transposable system for
692 gene delivery and lineage-specific differentiation in human embryonic stem cells. *Cell Stem Cell* **5**,
693 332–342 (2009).
694 52. Peng, T. *et al.* A BaSiC tool for background and shading correction of optical microscopy images. *Nat.*
695 *Commun.* **8**, 14836 (2017).
696 53. Preibisch, S., Saalfeld, S. & Tomancak, P. Globally optimal stitching of tiled 3D microscopic image
697 acquisitions. *Bioinforma. Oxf. Engl.* **25**, 1463–1465 (2009).
698 54. Schmidt, U., Weigert, M., Broaddus, C. & Myers, G. Cell Detection with Star-convex Polygons.
699 *arXiv.org* https://arxiv.org/abs/1806.03535v2 (2018) doi:10.1007/978-3-030-00934-2_30.
700 55. Ershov, D. *et al.* TrackMate 7: integrating state-of-the-art segmentation algorithms into tracking
701 pipelines. *Nat. Methods* **19**, 829–832 (2022).
702

703 **Acknowledgements**

704 We thank all members of the teams of Pascal Hersen and Jerome Collignon (IJM, PARIS) for fruitful
705 discussion throughout the project. We thank A.H. Brivanlou for providing the RUES2 and GLR hESC line, the
706 mechanical workshops of the MSC and PCC labs for design and fabrication of custom parts for the gradient
707 chip and Carine Vias at the BMBC platform for help with molecular biology. This work was funded by grants
708 from Agence Nationale de la Recherche (ANR-15-CE13-0007, ANR-23-CE13-0018), CNRS (emergence
709 INC2023), Labex CellInScale, Qlife and Human Frontier Science Program (HFSP CDA00063/2015-C). M. Q.
710 has benefitted from the support of ANR-18-CE13-0028-03 (GuideFusion) attributed to VH

711

Author contributions

Conceptualization, TW, MQ, PH, VH, BS; Methodology, TW, SB, PH, BS; Investigation, TW, MQ, JS, HO, SB, BS; Formal Analysis, TW, MQ, JS, GT, MQ, VH, BS; Writing, TW, MQ, JS,VH, BS; Supervision, VH, BS.

Competing interests

The authors declare no competing interests.